# A multiparameter fracture mechanics approach to plasticity-induced crack tip shielding

M. N. James
*Faculty of Science & Technology, University of Plymouth, Plymouth (UK)*
*Nelson Mandela Metropolitan University, Department of Mechanical Engineering, Port Elizabeth (South Africa)*
*mjames@plymouth.ac.uk; eann@egr.msu.edu*

Yanwei Lu, C. J. Christopher
*Faculty of Science & Technology, University of Plymouth, Plymouth (UK)*

E. A. Patterson
*Composite Vehicle Research Center, Michigan State University, East Lansing (USA)*

**ABSTRACT.** This paper presents an outline of the development, verification and application of a new model of crack tip stress fields in the presence of a plastic enclave around a growing fatigue crack. The approach taken rests on capturing the effects of the crack tip and crack wake plastic zones through elastic stress distributions applied at the elastic-plastic boundary. A Muskhelishvili complex potential extension to the Williams crack tip stress field is found for four stress parameters representing a *K*-stress, a *T*-stress, a crack retardation stress and a compatibility-induced shear stress at the elastic-plastic boundary. This model is validated via full field fitting to photoelastic stress fringe patterns, obtained from epoxy resin and polycarbonate specimens. It has also been extended to the strain fields measured in digital image correlation techniques, which allows its application to metallic alloys.

**KEYWORDS.** Crack tip stresses; Mathematical modelling; Plastic inclusion; Fracture mechanics parameters; Crack shielding.

## INTRODUCTION

The single parameter description of crack tip stresses based on the stress intensity factor *K*, has proven extremely useful in characterising fatigue crack growth and underpins the development of a defect-tolerant approach to life prediction. The identification of the influence of plasticity-induced crack tip shielding by Christensen [1] and Elber [2] some 40 years ago led to the concept of an effective range of stress intensity factor $\Delta K_{eff}$, which is lower than the applied nominal range of stress intensity factor $\Delta K$. Considerable controversy around plasticity-induced shielding mechanisms, their magnitudes and measurement, has prevented a full understanding being attained of the phenomenon [e.g. 3, 4]. It remains difficult to predict, a priori, the influence of crack plastic zones on growth rates, particularly under variable amplitude or spectrum loading, even for straightforward cases of uniaxial loading.
It has also become clear that the extent and shape of crack tip plasticity is affected by the *T*-stress, which is the second term in a Williams-type expansion of the crack tip stresses [5]. The *T*-stress is a non-singular, constant stress quantity parallel to the direction of crack extension under mode I loading [5]. Under small scale yielding conditions, the *T*-stress describes the effects of in-plane geometry and loading type (e.g. tension vs. bending) on plastic deformation around the crack tip and on the fracture process [6]. Finite element 3D modelling by Roychowdhury and Dodds [6] has indicated that the magnitude of the *T*-stress influences the closure process through two factors; the stationary crack opening displacement and the residual plastic deformation left in the wake of a steadily growing fatigue crack. They found that if

the *T*-stress was zero then plastic contraction in the thickness direction compensated primarily for permanent deformation in the direction normal to the crack plane; if it was negative then plastic contraction in the in-plane transverse direction (parallel to the crack) contributes the larger share of material flowing into the normal direction (transverse to the crack), and if it was positive then both the in-plane directions experienced permanent stretching and the thickness direction alone underwent plastic contraction.
Similar work by Kim et al [7] studied the stationary crack front fields in a thin elastic–plastic plate and varied the *T*–stress to modify the in-plane constraint level. Their analysis demonstrated a strong influence of *T*-stress on crack front stresses and deformation fields. The size of the near-tip plastic zone, both at the centre-plane and near the free surface, increased as the *T*-stress deviated from zero. A negative *T*-stress had a more pronounced influence on plastic deformation with the plastic zone spreading predominantly at an angle of about 45° with the forward direction of the crack plane. For positive *T*-stress, the plastic zone tilts backward at low load and spreads parallel to the crack both in the forward and the backward direction at higher loads. It is clearly necessary to take account of the *T*-stress in trying to understand plasticity deformation at a crack tip.

## CRACK TIP STRESS FIELDS IN THE PRESENCE OF PLASTICITY

Whilst a two parameter characterisation of crack tip stress fields can capture influences of the applied elastic field on local plastic deformation around the crack tip, it still leaves unanswered the question of how to account for the influences on the applied elastic field of the crack tip shielding arising from the generation of a plastic enclave and wake associated with a growing fatigue crack. Such influences include fracture surface contact during the lower part of an applied load cycle (crack closure) and compatibility-induced shear stresses at the elastic-plastic boundary. The latter stresses arise because plastic deformation is a constant volume process with a Poisson's ratio of 0.5, while regions undergoing elastic deformation have a Poisson's ratio of about 0.38 in polycarbonate, or 0.3 in metals.
The approach to this problem adopted in the work reported by Christopher et al [8-9] was to define elastic stress distributions acting on the cracked specimen that represent the occurrence of wake contact and the interfacial shear stress at the elastic-plastic boundary. A complex potential Muskhelishvili stress analysis of the crack was then performed to solve for an applied stress perpendicular to the crack, the *T*-stress induced by the crack, the wake contact stress (taken to be a distribution which decays with an $r^{-1/2}$ dependence acting along the crack flank) and a compatibility-induced shear stress parallel to the crack. The mathematical model can generate full-field fringe patterns for stress in the presence of a crack subject to these stress components, which can be compared with experimentally generated full field fringe patterns.
In photoelasticity, the isochromatic fringe pattern gives lines along which the principal stress difference is equal to a constant. The stress equation is hence solved to provide the difference in principal stresses which allows a direct comparison to be made between an experimentally obtained full-field photoelastic fringe pattern and a mathematically derived full-field fringe pattern [10]. Values of the constants in the theoretical equation can therefore be obtained and the error in the fit can be calculated. The experimental photoelastic fringe patterns were obtained using 2 mm thick compact tension (CT) specimens of polycarbonate, which exhibits birefringence, continuum fatigue crack growth mechanisms over a range of crack growth rates, and ductile crack tip deformation by crazing which is analogous to the Dugdale strip yield plastic zone model [11, 12].
Full details of the mathematical technique are given in reference 8, and only the resulting equation is given below:

$$\frac{Nf}{h} = \left|\sigma_y - \sigma_x + 2i\,\sigma_{xy}\right| = \left|Gz^{-1/2} + Hz^{-3/2}\bar{z} + Cz^{0} + Dz^{-1/2}\ln\frac{z}{z_0} + Ez^{-3/2}\bar{z}\ln\frac{z}{z_0}\right| \qquad (1)$$

where *N* is fringe order number, *f* is known as the material fringe constant (typically 0.007 MPam/fringe for polycarbonate) and *h* is the specimen thickness. The terms in $z^{-1/2}$ provide a contribution to the stress field that becomes singular, i.e. the stress traditionally used to calculate a stress intensity factor, and the term in $z^{0}$ provides a constant contribution to the stress, equivalent to the *T*-stress. The other terms describe crack retardation stress and the compatibility-induced interfacial shear stress. Specific conditions apply to the constants to give appropriate forms to the stress distributions.
These crack tip stress terms $\sigma_y$, $\sigma_x$, and $\sigma_{xy}$ can then be interpreted as representing a net tensile stress perpendicular to the crack, a net direct stress acting parallel to the crack and a net shear stress, all of which include effects of the elastic-plastic boundary stresses arising from the total plastic enclave associated with fatigue crack growth. In principle, this approach is

an attempt at an extension of the linear elastic stress intensity approach to account for known influences of the plastic enclave generated by fatigue crack growth; it captures some key attributes underlying the dichotomy of using a global elastic stress field parameter to characterise a crack growth phenomenon based on local plasticity.
Three stress intensity factors, which characterise plastic enclave influences through elastic stress distributions acting at the elastic-plastic boundary, can then be defined from these stress terms and interpreted in terms of their effect on a growing fatigue crack. There is a term equivalent to the classical $K_I$ which is obtained through evaluating $\sigma_y$ in the limit along the $\theta = 0$ line towards the crack tip in the negative direction (i.e. $x > 0$). This is denoted $K_F$ and represents the driving force for crack growth. It explicitly includes a contribution to the direct stresses in the $y$-direction arising from crack tip shielding, reflecting the influences of Poisson's ratio and compatibility at the elastic-plastic boundary:

$$K_F = \lim_{r\to 0}\left[\sqrt{2\pi r}\left(\sigma_y + 2E\ln\left(\frac{r}{r_0}\right)\right)\right] = \sqrt{\frac{\pi}{2}}(G - 3H - 8E) \qquad (2)$$

In the absence of shielding $E = 0$ and this expression simplifies to the classical definition of the stress intensity factor. Similarly, the stress intensity factor characterising the compatibility-induced interfacial shear stress at the elastic-plastic boundary can also be obtained through the limit process applied to $\sigma_{xy}$ along the crack flank (on the $y > 0$ face) towards the crack tip:

$$K_S = \lim_{r\to 0}(\sqrt{2\pi r}\,\sigma_{xy}) = -\sqrt{\frac{\pi}{2}}(G + H) \qquad (3)$$

Finally, a third stress intensity factor can be defined by using the limit of the direct stress parallel to and ahead of the crack tip, i.e. $y = 0$ and $x < 0$:

$$K_R = \lim_{r\to 0}(\sqrt{2\pi r}\,\sigma_x) = -(2\pi)^{3/2}E \qquad (4)$$

This stress intensity factor characterises the direct stress opposing or retarding the crack growth parallel to the plane of the crack. It includes influences of the wake contact stress because $\sigma_x$ and $\sigma_y$ are equal in magnitude at the crack flanks. Fig.1 shows the principal stresses around the crack at zero applied load arising from the plastic enclave, for a situation in which $K_R$ is acting alone.

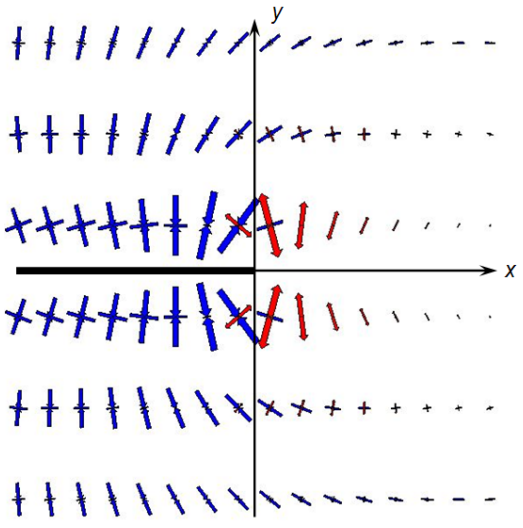


Figure 1: Principal stress field around the crack due to the presence of a plastic enclave leading to wake contact behind the crack tip. Blue indicates compressive stress and red indicates tensile stress. The crack is the thick horizontal line.

These new stress intensity factors have been derived from physically meaningful elastic stress distributions arising both from the applied load and from the plasticity generated by fatigue crack growth. They are therefore well suited to providing a better description of the elastic stress field surrounding a growing fatigue crack than has hitherto been

possible. As will be shown below, the full-field fit between experimentally obtained stress fringe patterns and those resulting from this model is closer than can be achieved using a two-parameter theoretical stress solution giving only $K_I$ and the *T*-stress.

## PHOTOELASTIC VERIFICATION OF THE MODEL

Christopher et al [8] verified the capability of the model to solve for the individual stress and stress intensity terms under static loading, before applying it characterisation of fatigue loading in polycarbonate specimens. The model was validated for a pure elastic case without *T*-stress, using a stress-frozen photoelastic slice of a photoelastic resin containing a 'static' crack; for a pure elastic case with *T*-stress using the photoelastic fringe pattern from a machined notch in a compact tension (CT) specimen; and for a crack with interfacial shear generated with a jeweller's saw in a polycarbonate CT specimen, in which the sawing process generated a plastic zone analogous to the plastic wake formed by fatigue crack growth. Fig.2 is reproduced from reference 8 and indicates the success of the mathematical model in replicating the experimentally observed fringe patterns for various types of crack in CT specimens.

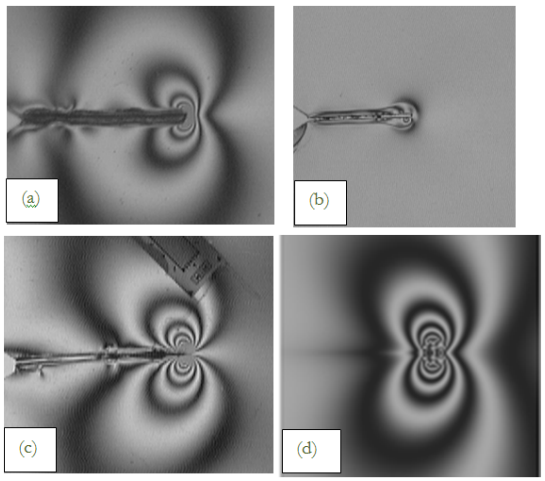


Figure 2: Fringe patterns in CT specimens generated by (a) a saw cut in a ductile polycarbonate specimen; (b) a saw cut in a brittle epoxy resin specimen; (c) applying the maximum load in a fatigue cycle to a propagating crack in a polycarbonate specimen. In addition (d) shows the result of fitting Eq. (1) to the photoelastic data for the saw cut in polycarbonate ($K_I$=0 MPa√m, $K_S$=0.22 MPa√m, $K_R$=-0.35 MPa√m and T-stress=2.4 MPa).

The photoelastic analysis is relatively complex, and uses the well established phase-stepping technique with masking of the regions surrounding the crack where plasticity is present. The size of these regions in a polycarbonate specimen can be estimated using the Dugdale strip yield model, where the plastic zone size ahead of the crack is given by:

$$r_P = \frac{\pi}{8}\left(\frac{K_I}{\sigma_{YS}}\right)^2 \qquad (5)$$

Confocal laser scanning (CLS) microscopy allows the plastic zone (equivalent to the crazed region) in polycarbonate specimens to be directly visualised and hence provides a check on the Dugdale plastic zone estimate and on the chosen mask size. This mask size is a key factor in ensuring that the model is fitted only to the elastic stress field driving crack growth and is not influenced by local plasticity around the crack. The generation of voids in the crazed region gives it a lower density and a lower refractive index, with void contents up to 45% reported in polycarbonate [13]. The change in refractive index can, in conjunction with the 3D imaging capability of modern CLS microscopes, provide images in which the crazed region is apparently elevated out of the surface as a contiguous block of material. Its width and extent ahead of the surface crack tip can then be easily measured.

Fig.3 demonstrates the utility of the approach for a polycarbonate CT specimen containing a crack of length 35 mm (a/W = 0.49) and subject to a nominal $K_{max}$ = 2.07 MPa√m. Fig.3a gives a standard optical image showing the photoelastic isochromatic fringes around the crack tip. It is difficult to detect the forward and lateral extent of the plastic zone in this

image. In contrast, Fig.3b taken using the CLS microscope clearly shows those regions around the crack where surface displacement has occurred; rotating this image, as in Fig.3c, demonstrates how the change in refractive index in the crazed material causes it to stand out from the uncrazed polymer. This indicates that the width of the crazed zone is some 0.61 mm at the craze tip, compared with a Dugdale estimate of 0.47 mm for forward extent of the plastic zone. The mask would be applied over a region at least twice the size of this width, i.e. some 1.2 mm.

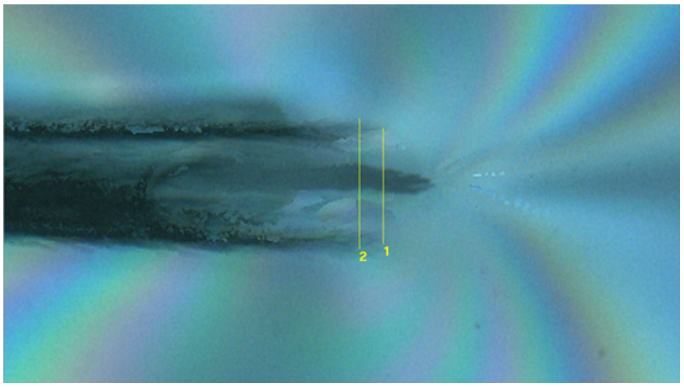


Figure 3a: Photoelastic isochromatic fringe patterns for a 35 mm crack in a polycarbonate CT specimen. It is hard to identify either the crack tip or the crazed region.

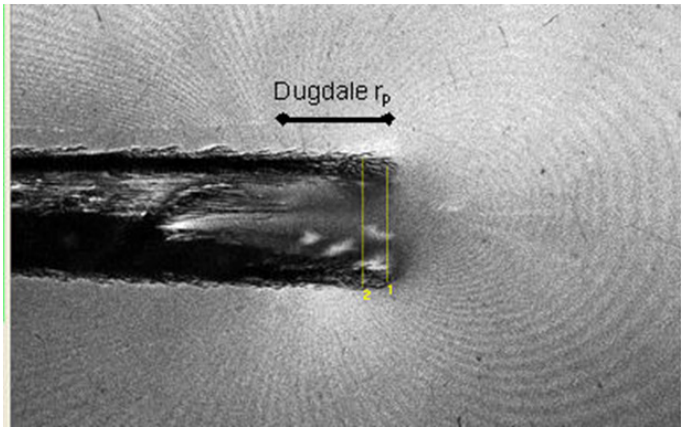


Figure 3b: CLS microscope image for a 35 mm crack in a polycarbonate CT specimen which clearly shows the craze extent. The Dugdale calculation indicates a plastic zone size ahead of 0.47 mm and the measured width using CLSM is 0.61 mm at the tip of the crazed region.

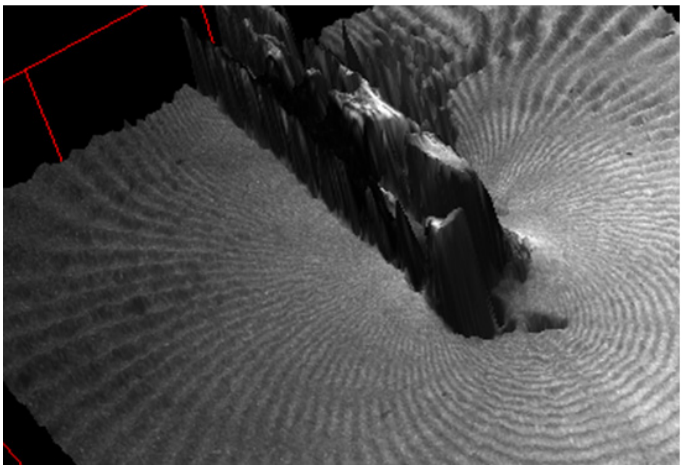

Figure 3c: Rotating the CLSM image allows clear visualisation of the manner in which the crazed region is 'lifted' out of the surface by the change in refractive index.

An interesting interference fringe pattern (Fizeau fringes [14]) can also be observed around the crack tip in Figgs. 3b and 3c, and arises because the confocal scanning laser microscope is being used in reflection and focussed progressively through the full depth of the specimen. Reflections from the top and bottom surface create an interference pattern that is related to the out-of-plane displacement at the surface, i.e. to the Poisson's contraction associated with the plastic zone. This is analogous to the output from the method of caustics and the change in direction of the fringe pattern behind the crack tip (from pointing forwards to pointing backwards) reflects the shear stress acting along the crack boundary.
Further verification of the new mathematical model for crack tip stresses in the presence of a plastic enclave derives from a full field comparison between experimentally derived photoelastic isoclinic fringe patterns and the equivalent fringe patterns obtained from the standard Williams solution with two stress parameters (*K*-stress and *T*-stress), and the new model with four stress parameters ($K_F$-stress, *T*-stress, $K_S$-stress and $K_R$-stress). These fits are shown in Fig.4 for near-crack tip fringes, along with the mean square root error of fringe order squared, calculated as:

$$Error = \sqrt{\frac{\sum (x - x_0)^2}{n}} \tag{6}$$

where $x$ is the theoretical fringe order, $x_0$ is the experimental fringe order and $n$ is the number of points considered (a matrix containing 54,602 points).

## MODEL DATA FOR FATIGUE CRACK GROWTH IN POLYCARBONATE

Typical data for the three stress intensity factor terms, $K_F$, $K_R$ and $K_S$, obtained from a 2 mm thick compact tension specimen of polycarbonate over a tensile half cycle of loading is shown in Fig.5. The nominal applied $K_I$ value is calculated using the standard expression [15]:

$$K_I = \frac{P}{BW^{0.5}} f\left(\frac{a}{W}\right) \tag{7}$$

where $B$ is the specimen thickness, $W$ is the distance from the loading line to the specimen edge along the direction of crack growth, $a$ is crack length and $P$ is the value of applied load.

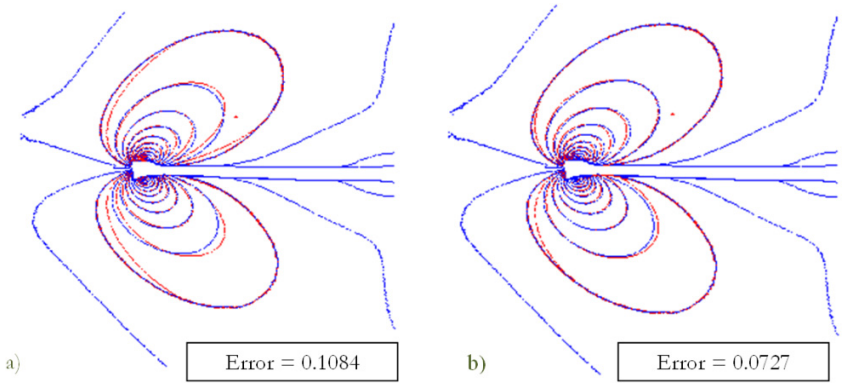


Figure 4: a) the standard 2-parameter Williams solution using K and T-stress; b) the new 4-parameter stress term model which incorporates two terms arising from plasticity-induced stresses. The red curves are the theoretical solution and the blue curves represent the experimental data.

The trends observed in the data can be interpreted in physically meaningful ways. Thus $K_F$ has a constant value of around 0.4 MPa√m until the nominal applied $K_I \approx 0.5$ MPa√m. $K_R$ is approximately zero and $K_S$ about -0.15 MPa√m up to the same point in the loading cycle. This can be interpreted as indicating that crack wake contact exists over the first 25% of the loading cycle. $K_F$ is lower than the nominal applied $K_I$ value, which is consistent with the occurrence of crack tip blunting, which is known to lead to lower values than the theoretical calculation, which assumes an infinitely sharp crack. The observed fairly linear decrease in $K_S$ once its value is > 0.6 MPa√m is likely to be related to the increasing Poisson's contraction as applied load increases. The $K_R$ and $K_S$ terms achieve magnitudes that are respectively 28% and 26% percent

of the nominal $K_I$ value which demonstrates the importance of the compatibility-induced stresses generated at the elastic-plastic boundary in fatigue crack growth. Further interpretation of the import of these parameters rests on additional experimental work, in particular an examination of the effects of stress ratio and overloads.

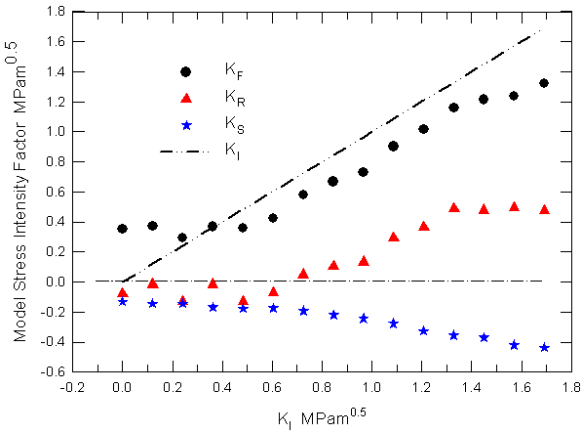


Figure 5: Typical output from applying the new model to full-filed photoelastic data. It shows the variation in the three new stress intensity factors through a tensile half cycle of loading.
Crack length a = 35 mm, R = 0.1 and $P_{max}$ = 120 N (equivalent to $K_{max}$ = 2.07 MPa√m).

## CONCLUSIONS

The work thus far has been focussed on several aspects:

1. Developing a more realistic mathematical model for crack tip stresses in the presence of a plastic 'inclusion' that imposes specific stresses at the elastic-plastic boundary.
2. Fitting the model to full-field experimentally-derived photoelastic data, which involves determining which regions of the stress field should be included in the solution for 'best' accuracy of fit.
3. Exploring the plastic zone size and crack growth mechanisms in polycarbonate to demonstrate that is a good model material for fatigue crack growth studies.
4. Extending the 4-parameter, 5-term mathematical model for crack tip stresses to displacements (strain) which allows digital image correlation to be done on metallic specimens.

Preliminary data, some of which has been presented in this paper, indicates that the approach gives a better fit between model and experimental data than is found using the traditional 2-parameter, 3-term Williams solution for crack tip stresses. Sensible trends are observed in the values of KF, KR, KS and T-stress found as a function of crack length, stress ratio R, and in the presence of an overload.

Future work will be aimed at improving the way in which the model captures effects of the plastic inclusion, and in exploring how to define stress and stress intensity parameters that provide the best predictive capability for characterising fatigue crack growth.

## REFERENCES

[1] R. H. Christensen, Appl. Mater. Res., 2(4) (1963) 207.
[2] W. Elber, Engng Fract. Mech., 2 (1970) 37.
[3] M. N. James in: Procs 9th Intl Conf. on Fract., Sydney, (eds. B L Karihaloo et al), Australia, Pergamon Press, 5 (1997) 2403.
[4] L.-W. Wei, M. N. James, Engng Fract. Mech., 66(2) (2000) 223.
[5] M. L. Williams, J. Appl. Mech., 24 (1957) 109.
[6] S. Roychowdhury, R. H. Dodds, Int. J. Solids Structs, 41 (2004) 2581.

[7] Y. Kim, X. K. Zhu, Y. J. Chao, Engng Fract. Mech., 68 (2001) 895.
[8] C. J. Christopher, M. N. James, E. A. Patterson, K. F. Tee, Int. J. Fract., 148 (2007) 361.
[9] C. J. Christopher, M. N. James, E. A. Patterson, K. F. Tee, Engng Fract. Mech., 75 (2008) 4190.
[10] A. D. Nurse, E. A. Patterson, Fatigue Fract. Engng Mater. Structs, 16(12) (1993) 1339.
[11] X. Li, H. A. Hristov, A. F. Yee, W. Gidley, Polymer, 36(4) (1995) 759.
[12] H. F. Brinson, Exp. Mech., 10 (1970) 72.
[13] R. P. Kambour, J. Polymer Sci. Part A: General Papers, 2(9) (1964) 4159.
[14] P. Hariharan, Optical Interferometry, 2nd Edition, Academic Press, New York (2003) 119.
[15] H. L. Ewalds, R. J. H. Wanhill, Fracture Mechanics, Arnold, London (1989).